Rydberg Atoms and Rydberg Quantum Gates

How Rydberg atoms are made, how they implement gates in neutral-atom arrays, and how results are read out

D. F. Hakala

October 2026

Table of Contents

1. Summary 2
2. What a Rydberg atom is 2
3. Preparing the qubits 3
4. Creating the Rydberg excitation 4
4.1 Excitation schemes 4
4.2 The driven Hamiltonian 5
4.3 Practical requirements 6
5. Interactions and blockade 6
6. Single-qubit gates 6
7. Rydberg multi-qubit gates: fourteen examples 7
7.1 Jaksch π–2π–π controlled-Z 8
7.2 Blockade CNOT and first entanglement (2010) 8
7.3 Global two-pulse CZ (Levine et al. 2019) 8
7.4 Time-optimal and smooth-pulse CZ gates 9
7.5 Adiabatic (rapid-passage) CZ gates 9
7.6 Rydberg-dressing gates 10
7.7 Three-qubit CCZ (Toffoli-class) gates 10
7.8 Multi-controlled C_kNOT and C_kZ gates 10
7.9 GHZ states and collective-blockade entanglers 10
7.10 Förster-resonance and dipole-exchange gates 11
7.11 Erasure-converting gates in alkaline-earth-like atoms 11
7.12 Ensemble (“superatom”) qubits and Fock-state preparation 11
7.13 Gates with atom transport and transversal logical gates 11
7.14 Analog blockade operations: PXP dynamics and maximum independent set 12
8. Reading out the result 12
9. Performance and error sources 13
10. Relevance to neutral-atom arrays and an LCoS-SLM tweezer design 14

References 14

1. Summary

A neutral-atom quantum computer stores each qubit in two long-lived ground-state levels of an atom held in an optical tweezer. The atoms barely interact in those states, which is why the qubits are stable, but it also means a gate needs a way to switch on a strong interaction for a short time. Rydberg states supply it. Laser excitation of one valence electron to a level with principal quantum number n ≈ 50–100 produces an atom roughly a micrometer across, with an interaction energy that varies as n^{11} and reaches tens of megahertz at 5 μm. When one atom is excited, the interaction shifts the doubly excited state of a nearby atom out of resonance, so the second atom cannot be excited. This **Rydberg blockade** [1–3] turns "is my neighbor excited?" into a conditional phase, which is all a controlled-Z (CZ) gate needs.

The sections below follow an atom through a computation:

- how the array is loaded and initialized (Section 3);
- how the Rydberg state is reached and what limits it (Section 4);
- how the interaction and blockade arise (Section 5);
- how single-qubit and Rydberg two- and multi-qubit gates are built, with fourteen worked examples (Sections 6 and 7);
- how results are read out (Section 8);
- current performance and error sources (Section 9);
- what this implies for an SLM-based tweezer system (Section 10).

A numerical simulation of the two main CZ protocols is included (Figure 4) to show how the pulse parameters produce the gate.

2. What a Rydberg atom is

A Rydberg atom has one electron in a highly excited level. For alkali atoms the energy follows a hydrogen-like formula with a quantum defect δ_ℓ that accounts for penetration of the inner-shell electrons:

$$E_{n\ell j} = E_\infty - \frac{R_M}{(n-\delta_{\ell j})^2} = E_\infty - \frac{R_M}{n^{*2}} \qquad (2.1)$$

where R_M is the mass-corrected Rydberg constant (109,736.6 cm^{-1} for ^{87}Rb) and n* the effective quantum number. For Rb $nS_{1/2}$ states δ ≈ 3.131, so $70S_{1/2}$ (n* = 66.87) lies 24.5 cm^{-1} (735 GHz) below the ionization limit [4, 5].

Because almost every property depends on a power of n*, the Rydberg level can be chosen to suit the gate (Figure 2a; Table 2.1).

Property	Scaling	Rb $70S_{1/2}$ (approximate)
Binding energy	n^{*-2}	24.5 cm^{-1} (735 GHz)
Orbital radius	n^{*2}	≈ 0.35 μm
Spacing between adjacent n	n^{*-3}	≈ 22 GHz
Transition dipole to neighboring states	n^{*2}	≈ 5000 e a_0
Radiative lifetime (0 K)	n^{*3}	≈ 400 μs
Lifetime including 300 K blackbody radiation	≈ n^{*2}	≈ 150 μs
Static polarizability (electric-field sensitivity)	n^{*7}	very large: stray fields of mV cm^{-1} shift the line by MHz
van der Waals coefficient C_6	n^{*11}	C_6/h ≈ 862 GHz $μm^6$

Table 2.1. Rydberg-state properties. Values for Rb $70S_{1/2}$ from Bernien et al. [6], Beterov et al. [7], and the ARC calculator [8].

The useful property for gates is the interaction (n^{*11}). The costs are finite lifetime (radiative decay and transitions driven by room-temperature blackbody radiation) and extreme sensitivity to electric fields, which is why Rydberg experiments use electrodes or careful shielding to null stray fields.

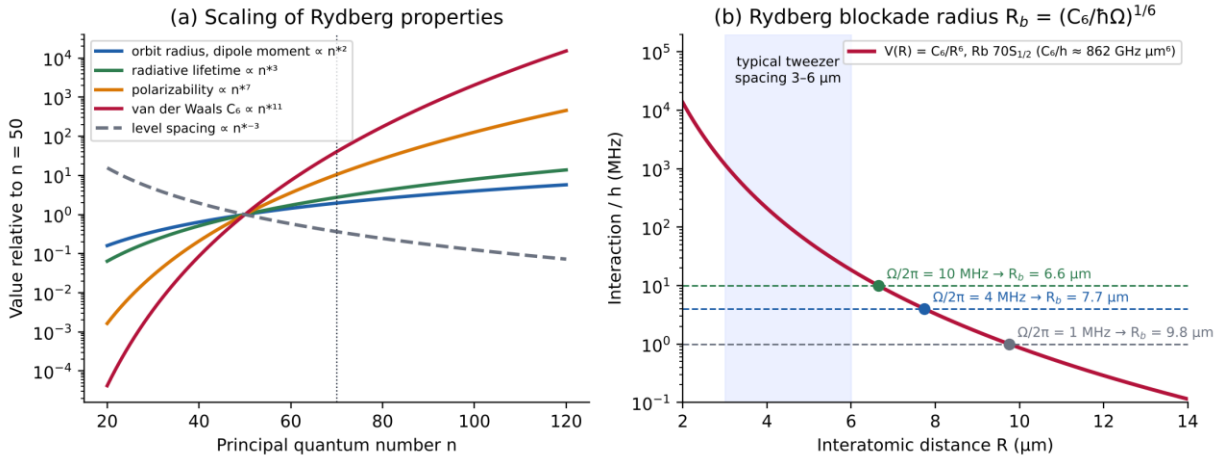


Figure 2. (a) Scaling of Rydberg properties with principal quantum number. (b) van der Waals interaction between two Rb $70S_{1/2}$ atoms against distance, with the blockade radius for three Rabi frequencies; typical tweezer spacings are shaded.

3. Preparing the qubits

Before any Rydberg excitation, the atoms are prepared in a defect-free array of ground-state qubits (Figure 5).

1. **Loading.** Atoms from a magneto-optical trap (MOT) are loaded into an array of optical tweezers, tightly focused beams far red-detuned from resonance (for Rb typically 800–1064

nm, depth about 1 mK). Light-assisted collisions in the small trap volume eject atoms in pairs, so each tweezer ends with zero or one atom, each with about 50% probability ("collisional blockade") [9].

2. **Imaging and rearrangement.** A fluorescence image shows which sites are filled. A second set of movable tweezers, steered by acousto-optic deflectors (AODs), then carries atoms into a defect-free target pattern [10, 11]. Arrays of 256 [12], about 1,000 [13], and several thousand atoms [14] have been assembled this way, and SLM-generated tweezer arrays are now standard for the static traps [15].
3. **Cooling.** Raman sideband cooling [16] or Λ-enhanced gray molasses reduces the motional energy, which matters because thermal motion produces Doppler shifts and position spread during Rydberg pulses.
4. **Initialization.** Optical pumping prepares every atom in one qubit state. For ^{87}Rb the usual qubit is the "clock" pair $|0\rangle = |F = 1, m_F = 0\rangle$ and $|1\rangle = |F = 2, m_F = 0\rangle$, split by 6.835 GHz and first-order insensitive to magnetic fields [17]. Alkaline-earth and alkaline-earth-like atoms (Sr, Yb) offer nuclear-spin qubits in the ground or metastable $^3P_0$ state [18–20], and some experiments use the ground and Rydberg states themselves as the qubit ("gr" qubit) [6, 21].

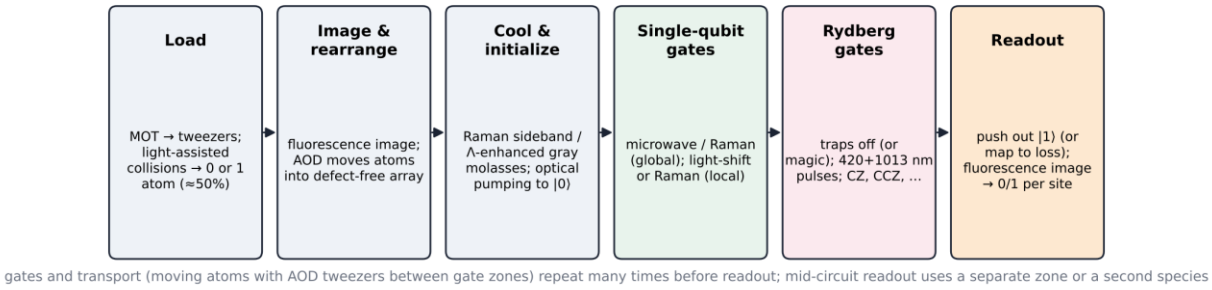


Figure 5. Operating cycle of a neutral-atom processor.

4. Creating the Rydberg excitation

4.1 Excitation schemes

The excitation is a coherent laser drive from one qubit state, normally $|1\rangle$, to a chosen Rydberg level $|r\rangle$. The transition from the ground state of Rb to nS or nD levels is near 297 nm, inconvenient for a single laser, so alkali experiments use a two-photon ladder through an intermediate P state, detuned by Δ to avoid populating it (Figure 1):

- **Rb via $5P_{3/2}$:** 780 nm + 480 nm. This was used in the early blockade and gate experiments [2, 22].
- **Rb via $6P_{3/2}$:** 420 nm + 1013 nm. The 420 nm leg has a smaller dipole matrix element, but the 6P state decays more slowly and 1013 nm light can be produced at high power, so larger single-photon Rabi frequencies and lower scattering are possible. This is the scheme used in the Harvard/QuEra processors [21, 23, 24].
- **Cs via $7P_{1/2}$:** 459 nm + 1038 nm (Wisconsin) [25, 26].

- **Sr and Yb:** a single UV photon from a metastable state, 317 nm from Sr 5s5p $^3P_1$ or $^3P_0$ and 302 nm from Yb $^3P_0$ [18, 19, 27].

With single-photon Rabi frequencies Ω_1 and Ω_2 and intermediate detuning $\Delta \gg \Omega_1, \Omega_2$, the intermediate state can be eliminated, leaving an effective two-level drive

$$\Omega = \frac{\Omega_1 \Omega_2}{2\Delta} \tag{4.1}$$

plus light shifts of the two levels, which are cancelled by adjusting the two-photon detuning. Off-resonant scattering from the intermediate state, with decay rate Γ_P, is the main incoherent error of the excitation. For a π pulse the scattering probability is (with Δ taken as its magnitude)

$$P_{sc} \approx \frac{\pi \Gamma_P}{4\Delta} \frac{\Omega_1^2 + \Omega_2^2}{\Omega_1 \Omega_2} \tag{4.2}$$

which is smallest, $\pi\Gamma_P/(2\Delta)$, when $\Omega_1 = \Omega_2$. Large Δ (1–7 GHz) and correspondingly high laser powers are therefore required. Typical effective Rabi frequencies are $\Omega/2\pi$ = 1–10 MHz, so a π pulse takes 50–500 ns.

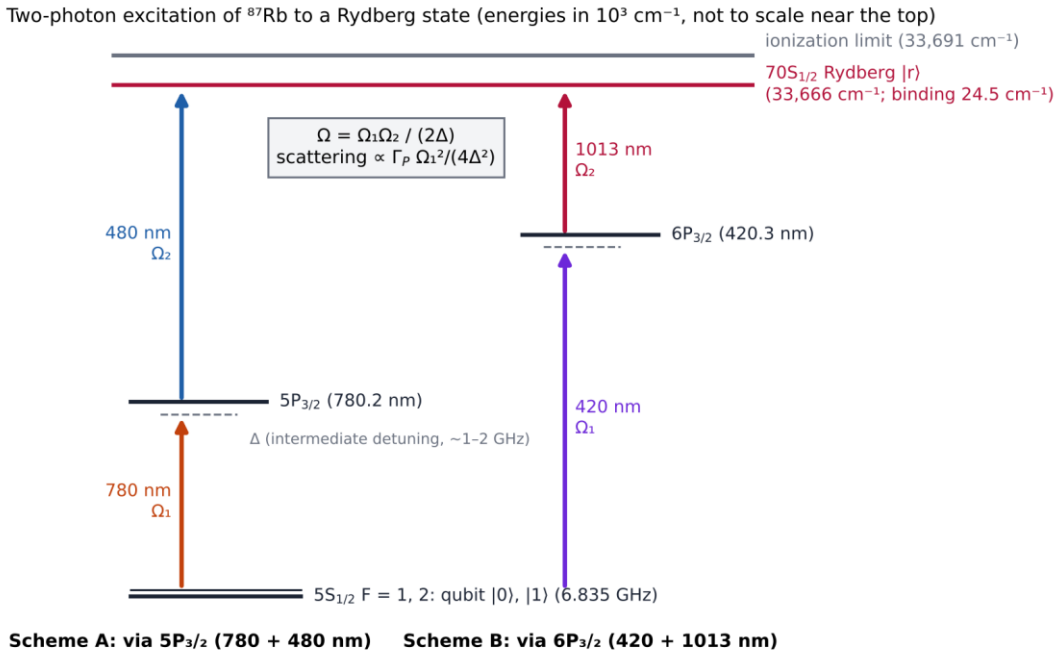


Figure 1. Two-photon excitation of ^{87}Rb from the qubit level to $70S_{1/2}$ by the two common ladders.

4.2 The driven Hamiltonian

For N atoms in the frame rotating with the lasers, the Rydberg drive and interaction give

$$H/\hbar = \Sigma_i \left[(\Omega_i/2)(e^{i\varphi i} |r\rangle_i\langle 1| + \text{h.c.}) - \Delta_i n_i \right] + \Sigma_{i<j} (V_{ij}/\hbar)\, n_i n_j,\ n_i = |r\rangle_i\langle r| \tag{4.3}$$

The state $|0\rangle$ is far off resonance and does not couple. Every Rydberg gate is a choice of the controls $\Omega_i(t)$, $\varphi_i(t)$, $\Delta_i(t)$, applied globally or to individual atoms, together with the atom positions that set V_{ij}.

4.3 Practical requirements

- **Trap switching.** Ground-state tweezers are repulsive for a Rydberg atom, whose nearly free electron sees a ponderomotive potential, so the tweezers are usually switched off for the 0.2–2 μs of the Rydberg pulses and switched back on before the atom moves appreciably [2, 21]. Ponderomotive "bottle" traps [28] and, for alkaline-earth atoms, the polarizable ion core [29] allow Rydberg atoms to be trapped.
- **Laser phase noise and intensity noise.** These translate directly into gate error. The lasers are locked to high-finesse cavities, and the cavity's transmission is often used as a filter to suppress high-frequency phase noise [23, 30].
- **Doppler and position effects.** Counter-propagating beams reduce the two-photon Doppler shift. Residual motion and position spread give shot-to-shot detuning and Rabi-frequency variations, which robust pulse shapes (Section 7.4) are designed to tolerate.
- **Electric and magnetic fields.** Stray fields must be nulled to the mV cm^{-1} level. A bias magnetic field defines the quantization axis and the Zeeman substructure of $|r\rangle$.

5. Interactions and blockade

Two Rydberg atoms at distance R interact through their large dipoles. When no Förster resonance is near, second-order dipole–dipole coupling gives a van der Waals interaction

$$V(R) = \frac{C_6}{R^6} \tag{5.1}$$

which for Rb $70S_{1/2}$ is h × 862 GHz μm^6 / R^6, or h × 55 MHz at 4 μm. Near a Förster resonance, where two pair states are nearly degenerate, the interaction becomes resonant dipole–dipole, C_3/R^3, and can be tuned with a small electric field [31].

If the interaction exceeds the excitation linewidth (ħΩ), the doubly excited state $|rr\rangle$ is shifted out of resonance and only one atom of the pair can be excited. The **blockade radius** is defined by $V(R_b) = \hbar\Omega$:

$$R_b = \left(\frac{C_6}{\hbar\Omega}\right)^{1/6} \tag{5.2}$$

For Rb 70S and $\Omega/2\pi$ = 4 MHz, $R_b \approx 7.7$ μm (Figure 2b), comfortably larger than typical tweezer spacings of 3–6 μm.

Under blockade, a pair starting in $|11\rangle$ is driven to the symmetric single-excitation state

$$|W\rangle = (|1r\rangle + |r1\rangle) / \sqrt{2} \tag{5.3}$$

with a collectively enhanced Rabi frequency $\sqrt{2}\,\Omega$; for N atoms within R_b the enhancement is $\sqrt{N}\,\Omega$ [1]. The $\sqrt{2}$ enhancement and the single-excitation limit were first observed with two atoms held 4 μm and 10 μm apart in 2009 [2, 3]. These two facts, a different Rabi frequency and a forbidden $|rr\rangle$, are what every blockade gate uses.

6. Single-qubit gates

A universal gate set needs arbitrary single-qubit rotations plus one entangling gate. Single-qubit gates act on the hyperfine or nuclear-spin qubit with no Rydberg excitation:

1. **Global microwave rotations.** A 6.8 GHz (Rb) or 9.2 GHz (Cs) field rotates all qubits at once. Randomized benchmarking gives errors near 10^{-4} [17, 32].
2. **Global or local two-photon Raman rotations.** A pair of laser beams detuned from the D lines, with frequency difference equal to the qubit splitting, drives the qubit optically. With tightly focused or AOD-scanned beams this addresses individual atoms [21, 24].
3. **Local Z rotations by light shifts.** A focused, off-resonant beam on one atom shifts its qubit frequency, so a global microwave pulse rotates only the shifted (or only the unshifted) atoms. Wang et al. used crossed addressing beams to perform targeted gates in a three-dimensional array [33]; Xia et al. used the same principle in two dimensions [32].
4. **Virtual Z gates.** Z rotations are applied by shifting the phase of all later pulses, at no cost in time or error.

7. Rydberg multi-qubit gates: fourteen examples

The sequence diagrams in Figure 3 and the simulation in Figure 4 illustrate the first three protocols. For each example the descriptions give how the gate is created, how the qubits are manipulated, and how its output is read.

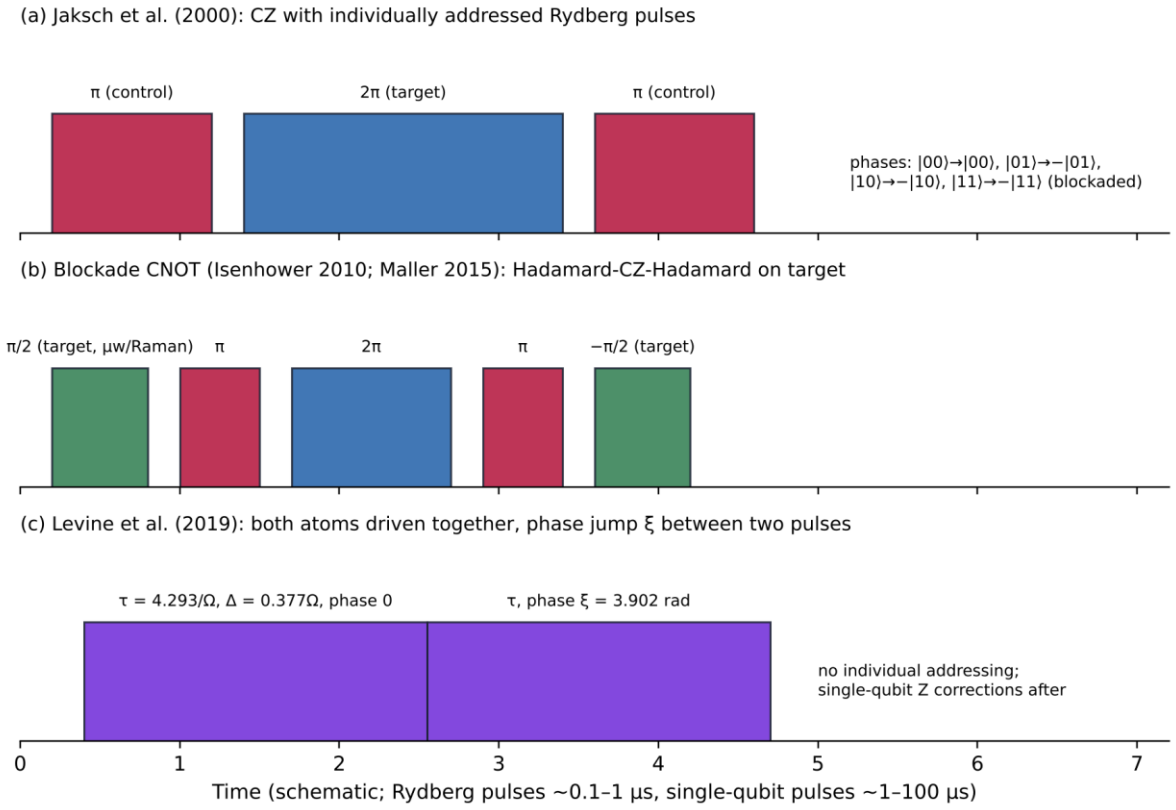


Figure 3. Pulse sequences for (a) the Jaksch π–2π–π CZ gate, (b) the blockade CNOT, and (c) the global two-pulse CZ of Levine et al.

7.1 Jaksch π–2π–π controlled-Z

Created by Jaksch et al. (2000) [1], the original Rydberg gate proposal. The control and target atoms are individually addressed by the Rydberg lasers.

Manipulation. (i) A π pulse on the control takes $|1\rangle_c \to |r\rangle_c$ (with a factor −i). (ii) A 2π pulse on the target takes $|1\rangle_t \to |r\rangle_t \to |1\rangle_t$, giving a sign change −1, unless the control is in $|r\rangle$, in which case the target is blockaded and nothing happens. (iii) A second π pulse returns the control. The four basis states acquire

$$|00\rangle \to |00\rangle,\ |01\rangle \to -|01\rangle,\ |10\rangle \to -|10\rangle,\ |11\rangle \to -|11\rangle \tag{7.1}$$

which is the controlled-Z gate

$$\mathrm{CZ} = \mathrm{diag}(1,1,1,-1) \tag{7.2}$$

up to single-qubit Z rotations on each atom. The simulation (Figure 4c) gives the error from imperfect blockade: about 4×10^{-3} at $V/\Omega = 10$, falling as $(\Omega/V)^2$. For ideal blockade, the error from Rydberg decay is approximately

$$\varepsilon_{decay} \approx \frac{7\pi}{4\,\Omega\,\tau_r} \tag{7.3}$$

where τ_r is the Rydberg lifetime [4, 34]. With $\Omega/2\pi = 5$ MHz and $\tau_r = 150$ μs this is about 2×10^{-4}.

Read out by applying the gate in a circuit (for example, Hadamard on the target, CZ, Hadamard) to produce a Bell state, then measuring both atoms in several bases (Section 8). Parity oscillations give the entanglement fidelity.

7.2 Blockade CNOT and first entanglement (2010)

Created by Isenhower et al. (Wisconsin, Rb, 8.7 μm spacing) [22] and Wilk et al. (Institut d'Optique, Rb, 4 μm) [35], both in 2010, the first neutral-atom entangling operations.

Manipulation. CNOT is obtained from CZ by Hadamard-like π/2 rotations on the target:

$$\mathrm{CNOT} = (I \otimes H)\,\mathrm{CZ}\,(I \otimes H) \tag{7.4}$$

The Wisconsin group used Raman π/2 pulses on the target around the π–2π–π sequence (Figure 3b). Wilk et al. instead excited both atoms with a global π pulse under blockade, producing the entangled state $(|r1\rangle + |1r\rangle)/\sqrt{2}$, then mapped $|r\rangle$ back to the second hyperfine level with a second laser, giving a ground-state Bell state. Maller et al. extended the CNOT to a two-dimensional 7 × 7 array with any pair of atoms selectable [25].

Read out with state-selective push-out and fluorescence: Isenhower et al. measured the CNOT truth table with fidelity 0.73 and created entanglement with fidelity 0.48 (0.58 after correcting for atom loss). Wilk et al. obtained 0.46 (0.75 after correction for loss).

7.3 Global two-pulse CZ (Levine et al. 2019)

Created by Levine et al. (Harvard) [21], who removed the need to address atoms individually during the gate.

Manipulation. Both atoms are driven together with a Rydberg laser detuned by $\Delta = 0.377\Omega$ for a time $\tau = 4.293/\Omega$. The laser phase is then jumped by $\xi = 3.902$ rad and a second identical pulse

applied. Under blockade, |01⟩ and |10⟩ undergo detuned Rabi oscillation at Ω, while |11⟩ oscillates to |W⟩ at $\sqrt{2}\,\Omega$ (Figure 4a). The parameters are chosen so that every state returns to the qubit subspace (closed trajectories, Figure 4b) and the phases satisfy

$$\phi_{11} = 2\phi_{01} + \pi \tag{7.5}$$

so that, after a single-qubit Z rotation by $-\varphi_{01}$ on each atom, the gate is CZ. The numerical simulation of the protocol (Figure 4) recovers $\tau\Omega = 4.29268$ and $\xi = 3.90242$ rad by optimizing for Equation 7.5 at $\Delta/\Omega = 0.377371$, matching the published values. With perfect blockade the result is exact. Levine et al. measured a CZ fidelity of 97.4% and also demonstrated a three-qubit CCZ gate (Section 7.7).

Read out: Bell-state fidelity from populations and parity oscillations after the gate.

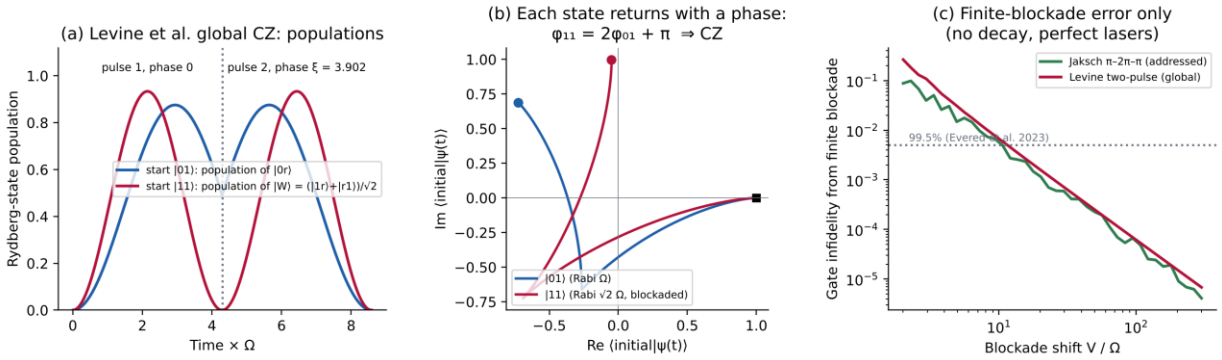


Figure 4. Simulation of the Levine et al. CZ protocol. (a) Rydberg populations for the initial states |01⟩ and |11⟩; (b) trajectories of the amplitude of the initial state, which both return to the unit circle with phases satisfying Equation 7.5; (c) gate error from finite blockade for this protocol and for the Jaksch protocol (no decay or laser noise).

7.4 Time-optimal and smooth-pulse CZ gates

Created by Jandura and Pupillo (2022) [36], who used optimal control to find the shortest global, phase-modulated pulse that implements CZ (total duration about 7.6/Ω, against 8.6/Ω for the two-pulse gate, with less time spent in |r⟩). Evered et al. (2023) implemented a smooth version on 60 atoms in parallel and reached a CZ fidelity of 99.5% [23], the first neutral-atom entangling gate at the threshold of surface-code error correction. Analytic shaped pulses that are robust to amplitude and detuning errors have also been proposed and analyzed [37, 38].

Manipulation. A single continuous pulse of constant amplitude with a smoothly varying laser phase φ(t), applied globally to all pairs inside the Rydberg zone. Pairs separated by much more than R_b are unaffected, so many gates run at once.

Read out: randomized benchmarking-style sequences of many CZ gates interleaved with random single-qubit gates, with the final state read by fluorescence; the decay of the return probability with sequence length gives the error per gate.

7.5 Adiabatic (rapid-passage) CZ gates

Created by Saffman et al. (2020) [39] in theory and Graham et al. (2019, Cs, in a 2D array) [26]. Chirped or amplitude-shaped pulses sweep through resonance adiabatically.

Manipulation. A symmetric pair of adiabatic rapid-passage pulses applied to both atoms returns each state with a dynamical phase that depends on whether the pair is blockaded. The adiabatic

sweep tolerates variations in Rabi frequency (laser intensity or position) and in detuning (Doppler shifts). Graham et al. used this approach to entangle pairs of Cs atoms across a two-dimensional array [26].

Read out: as for Section 7.3.

7.6 Rydberg-dressing gates

Created by Jau et al. (2016, Sandia, Cs) [40]. The ground state is weakly admixed with the Rydberg state by a far-detuned laser, so the atoms never fully enter $|r\rangle$.

Manipulation. A laser detuned by $\Delta \gg \Omega$ from the Rydberg transition gives each atom a small Rydberg admixture $(\Omega/2\Delta)^2$, and two dressed atoms interact through a soft-core potential

$$U(R) = \frac{\hbar\Omega^4}{8\Delta^3}\,\frac{1}{1+(R/R_c)^6}, \qquad R_c = \left(\frac{C_6}{2\hbar\Delta}\right)^{1/6} \tag{7.6}$$

which is flat for $R < R_c$. Holding the dressing on for a time T_d gives the pair a conditional phase $U_0 T_d/\hbar$; setting it to π yields CZ. Jau et al. observed this and entangled two atoms with fidelity 0.81 by an adiabatic dressing pulse. Dressing gates are slower and more exposed to decay than blockade gates, but they suit analog simulation of spin models and spin squeezing [41].

Read out: by fluorescence detection, giving correlations and Bell-state fidelity.

7.7 Three-qubit CCZ (Toffoli-class) gates

Created by Levine et al. (2019) [21] for three atoms in a line, all within one blockade radius. Graham et al. (2022, Wisconsin) used a C_2Z gate in algorithms [24].

Manipulation. The outer atoms (controls) and the middle atom (target) are driven so that the target acquires a π phase only when both controls are in $|1\rangle$. Levine et al. used a single global smooth pulse optimized for the three-atom blockade structure, plus individually addressed pulses on the middle atom. A Toffoli (CCNOT) follows by adding Hadamard rotations on the target.

Read out: truth-table measurement in the computational basis and phase measurement through GHZ-type parity; Levine et al. reported a truth-table fidelity of about 87%.

7.8 Multi-controlled C_kNOT and C_kZ gates

Created by Isenhower, Saffman, and Mølmer (2011) in theory [42]; Graham et al. demonstrated multi-qubit C_kZ gates in a processor [24].

Manipulation. Each of k control atoms receives a π pulse to $|r\rangle$ if it is in $|1\rangle$. A single target 2π pulse then succeeds only if no control is excited, because one excited control blockades it. The controls are returned with π pulses. All atoms must lie within a single blockade radius of the target, which limits k to a few with van der Waals interactions.

Read out: truth table in the computational basis.

7.9 GHZ states and collective-blockade entanglers

Created by Omran et al. (2019, Harvard) [43], who prepared Greenberger–Horne–Zeilinger (GHZ) states of up to 20 atoms.

Manipulation. An adiabatic sweep of the global detuning in a one-dimensional chain with nearest-neighbor blockade carries the system into the antiferromagnetic superposition $(|1010\ldots\rangle + |0101\ldots\rangle)/\sqrt{2}$. An optimized, high-speed version of the sweep reduces the time spent in Rydberg states.

Read out: the parity of all atoms after a global rotation; the oscillation of parity with rotation phase gives the GHZ coherence. Omran et al. obtained fidelities above 0.5, proving genuine multi-partite entanglement, for 20 atoms.

7.10 Förster-resonance and dipole-exchange gates

Created by Ravets et al. (2014) [31], with related gate proposals by Beterov et al. An electric field tunes two pair states into resonance, for example nD + nD ↔ (n+2)P + (n−2)F, turning the van der Waals interaction into a resonant C_3/R^3 interaction.

Manipulation. Switching the field on and off controls the interaction strength and its angular dependence. Ravets et al. observed coherent pair-state oscillations between the two pair states, which can be used to make a controlled phase on a precise time scale.

Read out: state-selective detection of the Rydberg state, for example by ionizing or by mapping to ground-state loss.

7.11 Erasure-converting gates in alkaline-earth-like atoms

Created by Ma et al. (2023, Princeton, ^{171}Yb) [19] and Scholl et al. (2023, Caltech, ^{88}Sr) [20].

Manipulation. The qubit is stored in metastable levels (nuclear spin of Yb $^3P_0$, or the Sr $^3P_0$ clock state). Rydberg gates use a single UV photon from the metastable state. Most Rydberg decays leave the atom in states outside the qubit subspace that can be detected separately without disturbing the qubits ("erasure conversion"). Known erasures are much easier for error correction to handle than unknown errors.

Read out: a fast fluorescence check of the ground state flags erasures mid-circuit; qubit states are then read by state-selective imaging. Ma et al. reached a CZ fidelity of 0.980, with about a third of the errors detected as erasures. Scholl et al. reported Bell-state fidelity of 0.9971 after excluding detected erasures.

7.12 Ensemble ("superatom") qubits and Fock-state preparation

Created by Lukin et al. (2001) [44] in theory; Ebert et al. (2014, 2015, Wisconsin) [45, 46] in experiment.

Manipulation. N atoms within one blockade volume share at most one Rydberg excitation, so the ensemble behaves as a two-level system with collective Rabi frequency $\sqrt{N}\,\Omega$. Ebert et al. used this to prepare atomic Fock states (exactly one atom transferred to the second hyperfine level) and to make ensemble qubits with blockade-controlled coherence.

Read out: counting the transferred atoms by state-selective fluorescence; Rabi oscillations with $\sqrt{N}$-enhanced frequency confirm blockade.

7.13 Gates with atom transport and transversal logical gates

Created by Bluvstein et al. (2022, 2024, Harvard/QuEra) [47, 48].

Manipulation. Atoms are carried by AOD tweezers between a storage zone and an entangling zone while preserving their hyperfine coherence. In the entangling zone, pairs are brought within R_b and a single global CZ pulse entangles every pair at once. Re-arranging which atoms are paired between pulses gives arbitrary connectivity. For error-corrected logical qubits, the same CZ applied between corresponding physical qubits of two code blocks is a transversal logical CNOT/CZ; with this, 48 logical qubits were operated and logical GHZ states, entangled logical Bell pairs, and logical magic states were demonstrated.

Read out: mid-circuit by moving ancilla atoms to a separate readout zone and imaging them without disturbing data qubits; at the end, by imaging all atoms. Correlated decoding of the logical measurements uses all syndrome information [49].

7.14 Analog blockade operations: PXP dynamics and maximum independent set

Created by Bernien et al. (2017) [6] and Ebadi et al. (2021, 2022) [12, 50].

Manipulation. The whole array is driven globally under Equation 4.3 with time-dependent $\Omega(t)$ and $\Delta(t)$. Blockade forbids neighboring excitations, giving the "PXP" constrained model. Adiabatic sweeps prepare the ground states of the blockade Hamiltonian; on unit-disk graphs these encode maximum independent sets (MIS), the basis of QuEra's optimization demonstrations. This is an analog, not gate-based, use of the same physics.

Read out: snapshots of the Rydberg-state populations. Atoms in $|r\rangle$ are lost when the tweezers turn back on (they are anti-trapped and ionized), so a missing atom in the final image means "excited" [6, 12].

8. Reading out the result

The output of a neutral-atom computation is a set of fluorescence images.

1. **State-selective loss plus fluorescence (standard).** A resonant "push-out" beam on the $|F = 2\rangle \rightarrow |F' = 3\rangle$ cycling transition heats atoms in $|1\rangle$ out of their traps, leaving only atoms in $|0\rangle$. Imaging then shows a bright site for $|0\rangle$ and a dark site for $|1\rangle$ (or the reverse, by first swapping the states). Detection fidelity is typically 98–99.5%, limited mostly by atom loss during imaging and push-out imperfections [17, 21].
2. **Loss-based Rydberg detection.** For analog experiments and diagnostics, atoms left in $|r\rangle$ when the tweezers return are expelled, so absence of fluorescence means $|r\rangle$ [6].
3. **Non-destructive, state-selective imaging.** Imaging on a cycling transition while the other qubit state is shelved far off resonance keeps the atom in its trap, so it can be reused without reloading [51].
4. **Mid-circuit measurement.** Measuring some qubits while others continue requires protecting the data qubits from scattered imaging light. This is done by moving ancillas to a separate zone [48], by using two species with very different transition wavelengths, or, in alkaline-earth-like atoms, by shelving data qubits in a metastable state ("omg" architecture) while ground-state ancillas are imaged [52, 53].
5. **Erasure detection.** Fast checks for atoms that have left the qubit subspace, as in Section 7.11 [19, 20].

The images are converted to bit strings site by site by thresholding photon counts from an EMCCD or qCMOS camera, and repeated runs give probabilities and correlations from which gate fidelities and algorithm outputs are computed.

9. Performance and error sources

Year	Gate or operation	Group, atom	Fidelity	Reference
2009	Blockade of two atoms observed	Wisconsin (Rb); Institut d'Optique (Rb)	–	[2, 3]
2010	CNOT / Bell state	Wisconsin (Rb)	0.73 (truth table); 0.48 Bell	[22]
2010	Bell state by blockade	Institut d'Optique (Rb)	0.46 (0.75 loss-corrected)	[35]
2016	Dressing-induced entanglement	Sandia (Cs)	0.81	[40]
2019	Global CZ; CCZ	Harvard (Rb)	0.974; ≈0.87	[21]
2019	Adiabatic CZ in 2D array	Wisconsin (Cs)	entanglement demonstrated	[26]
2020	Bell state, Sr Rydberg	Caltech (Sr)	0.991 (SPAM-corrected)	[27]
2022	CZ, C_2Z, algorithms (GHZ, Grover, phase estimation)	Wisconsin/ColdQuanta (Cs)	see reference	[24]
2023	Parallel time-optimal CZ, 60 atoms	Harvard/MIT/QuEra (Rb)	0.995	[23]
2023	CZ with erasure conversion	Princeton (Yb)	0.980	[19]
2023	Bell state with erasure excision	Caltech (Sr)	0.9971	[20]
2024	48 logical qubits, transversal gates	Harvard/QuEra (Rb)	–	[48]

Table 9.1. Milestones in Rydberg gates. Fidelity definitions differ between groups (gate versus Bell state, raw versus corrected); see the references for details.

The main error sources of current Rydberg CZ gates, roughly in order of importance, are:

1. **Laser phase and intensity noise**, causing dephasing and Rabi-frequency errors during the gate [30].
2. **Rydberg-state decay**, radiative and blackbody-induced (Equation 7.3), which favors fast gates (large Ω).
3. **Intermediate-state scattering** in two-photon schemes (Equation 4.2), which favors large Δ and therefore high laser power.

4. **Finite blockade** (Figure 4c), which favors close spacing or higher n.
5. **Doppler shifts and position spread**, which favor cooling and robust pulse shapes.
6. **Atom loss and leakage** out of the qubit subspace, which can be converted to detected erasures in Yb and Sr.

10. Relevance to neutral-atom arrays and an LCoS-SLM tweezer design

Most of the points above translate directly into design requirements for a neutral-atom tweezer system based on LCoS spatial light modulators.

1. **Site spacing versus blockade radius.** Gates need $R < R_b$ for the pairs that interact and $R \gg R_b$ for the pairs that must not. With Rb 70S and $\Omega/2\pi \approx 5$ MHz ($R_b \approx 7.5$ μm), interacting pairs are placed at about 2–3 μm and non-interacting sites more than about 10 μm apart, since the interaction at $2R_b$ is still $\Omega/64$. An SLM hologram can produce both spacings in different zones of one array (storage and entangling zones, as in Section 7.13).
2. **SLM for static traps, AODs for motion.** The LCoS frame rate (60 Hz–1 kHz) is too slow for moving atoms during a circuit. The usual architecture uses SLM holograms for the static array and AOD tweezers to carry atoms into gate positions. SLM phase-pattern accuracy determines trap-depth uniformity, which affects light shifts and therefore gate detuning.
3. **Trap-off timing.** Because tweezers switch off during Rydberg pulses, the tweezer light must be modulated in under about 1 μs. An SLM cannot do this; an AOM or EOM upstream of the SLM switches the whole array.
4. **Uniform Rydberg illumination.** Global gates (Sections 7.3–7.4) need nearly equal Ω at every pair. Flat-top shaping of the 420 nm and 1013 nm beams, which can itself be done with an SLM or a fixed diffractive element, reduces Rabi-frequency variation across the array.
5. **Local addressing.** Light-shift addressing (Section 6) can use a second SLM- or AOD-generated pattern of focused beams; an SLM gives arbitrary static patterns, an AOD fast reconfiguration.
6. **Polarization and wavelength.** LCoS SLMs modulate one linear polarization and have limited damage thresholds. High-power 1013 nm and 420 nm beams, and tweezer powers of tens of watts for thousands of sites, require SLMs rated for that power and wavelength, with thermal management.
7. **Electric-field environment.** Rydberg states are very sensitive to stray fields. LCoS devices and their electronics placed near the vacuum cell can be a source of field noise, so the SLM should sit well outside the cell with field electrodes around the atoms.

References

1. D. Jaksch, J. I. Cirac, P. Zoller, S. L. Rolston, R. Côté, and M. D. Lukin, "Fast quantum gates for neutral atoms," *Phys. Rev. Lett.* **85**, 2208 (2000).
2. E. Urban, T. A. Johnson, T. Henage, L. Isenhower, D. D. Yavuz, T. G. Walker, and M. Saffman, "Observation of Rydberg blockade between two atoms," *Nat. Phys.* **5**, 110 (2009).

3. A. Gaëtan, Y. Miroshnychenko, T. Wilk, A. Chotia, M. Viteau, D. Comparat, P. Pillet, A. Browaeys, and P. Grangier, "Observation of collective excitation of two individual atoms in the Rydberg blockade regime," *Nat. Phys.* **5**, 115 (2009).
4. M. Saffman, T. G. Walker, and K. Mølmer, "Quantum information with Rydberg atoms," *Rev. Mod. Phys.* **82**, 2313 (2010).
5. T. F. Gallagher, *Rydberg Atoms* (Cambridge University Press, 1994).
6. H. Bernien et al., "Probing many-body dynamics on a 51-atom quantum simulator," *Nature* **551**, 579 (2017).
7. I. I. Beterov, I. I. Ryabtsev, D. B. Tretyakov, and V. M. Entin, "Quasiclassical calculations of blackbody-radiation-induced depopulation rates and effective lifetimes of Rydberg nS, nP, and nD alkali-metal atoms with n ≤ 80," *Phys. Rev. A* **79**, 052504 (2009).
8. N. Šibalić, J. D. Pritchard, C. S. Adams, and K. J. Weatherill, "ARC: An open-source library for calculating properties of alkali Rydberg atoms," *Comput. Phys. Commun.* **220**, 319 (2017).
9. N. Schlosser, G. Reymond, I. Protsenko, and P. Grangier, "Sub-poissonian loading of single atoms in a microscopic dipole trap," *Nature* **411**, 1024 (2001).
10. M. Endres et al., "Atom-by-atom assembly of defect-free one-dimensional cold atom arrays," *Science* **354**, 1024 (2016).
11. D. Barredo, S. de Léséleuc, V. Lienhard, T. Lahaye, and A. Browaeys, "An atom-by-atom assembler of defect-free arbitrary two-dimensional atomic arrays," *Science* **354**, 1021 (2016).
12. S. Ebadi et al., "Quantum phases of matter on a 256-atom programmable quantum simulator," *Nature* **595**, 227 (2021).
13. L. Pause, T. Preuschoff, D. Schäffner, M. Schlosser, and G. Birkl, "Supercharged two-dimensional tweezer array with more than 1000 atomic qubits," *Optica* **11**, 222 (2024).
14. N.-C. Chiu et al., "Continuous operation of a coherent 3,000-qubit system," *Nature* (2025).
15. D. Barredo, V. Lienhard, S. de Léséleuc, T. Lahaye, and A. Browaeys, "Synthetic three-dimensional atomic structures assembled atom by atom," *Nature* **561**, 79 (2018); A. M. Kaufman and K.-K. Ni, "Quantum science with optical tweezer arrays of ultracold atoms and molecules," *Nat. Phys.* **17**, 1324 (2021).
16. A. M. Kaufman, B. J. Lester, and C. A. Regal, "Cooling a single atom in an optical tweezer to its quantum ground state," *Phys. Rev. X* **2**, 041014 (2012).
17. M. Saffman, "Quantum computing with atomic qubits and Rydberg interactions: progress and challenges," *J. Phys. B* **49**, 202001 (2016).
18. S. Ma et al., "Universal gate operations on nuclear spin qubits in an optical tweezer array of ^{171}Yb atoms," *Phys. Rev. X* **12**, 021028 (2022).
19. S. Ma et al., "High-fidelity gates and mid-circuit erasure conversion in an atomic qubit," *Nature* **622**, 279 (2023).
20. P. Scholl et al., "Erasure conversion in a high-fidelity Rydberg quantum simulator," *Nature* **622**, 273 (2023).
21. H. Levine et al., "Parallel implementation of high-fidelity multiqubit gates with neutral atoms," *Phys. Rev. Lett.* **123**, 170503 (2019).

22. L. Isenhower, E. Urban, X. L. Zhang, A. T. Gill, T. Henage, T. A. Johnson, T. G. Walker, and M. Saffman, "Demonstration of a neutral atom controlled-NOT quantum gate," *Phys. Rev. Lett.* **104**, 010503 (2010).

23. S. J. Evered et al., "High-fidelity parallel entangling gates on a neutral-atom quantum computer," *Nature* **622**, 268 (2023).

24. T. M. Graham et al., "Multi-qubit entanglement and algorithms on a neutral-atom quantum computer," *Nature* **604**, 457 (2022).

25. K. M. Maller, M. T. Lichtman, T. Xia, Y. Sun, M. J. Piotrowicz, A. W. Carr, L. Isenhower, and M. Saffman, "Rydberg-blockade controlled-NOT gate and entanglement in a two-dimensional array of neutral-atom qubits," *Phys. Rev. A* **92**, 022336 (2015).

26. T. M. Graham et al., "Rydberg-mediated entanglement in a two-dimensional neutral atom qubit array," *Phys. Rev. Lett.* **123**, 230501 (2019).

27. I. S. Madjarov et al., "High-fidelity entanglement and detection of alkaline-earth Rydberg atoms," *Nat. Phys.* **16**, 857 (2020).

28. D. Barredo, V. Lienhard, P. Scholl, S. de Léséleuc, T. Boulier, A. Browaeys, and T. Lahaye, "Three-dimensional trapping of individual Rydberg atoms in ponderomotive bottle beam traps," *Phys. Rev. Lett.* **124**, 023201 (2020).

29. J. T. Wilson, S. Saskin, Y. Meng, S. Ma, R. Dilip, A. P. Burgers, and J. D. Thompson, "Trapping alkaline earth Rydberg atoms in optical tweezer arrays," *Phys. Rev. Lett.* **128**, 033201 (2022).

30. S. de Léséleuc, D. Barredo, V. Lienhard, A. Browaeys, and T. Lahaye, "Analysis of imperfections in the coherent optical excitation of single atoms to Rydberg states," *Phys. Rev. A* **97**, 053803 (2018).

31. S. Ravets, H. Labuhn, D. Barredo, L. Béguin, T. Lahaye, and A. Browaeys, "Coherent dipole–dipole coupling between two single Rydberg atoms at an electrically-tuned Förster resonance," *Nat. Phys.* **10**, 914 (2014).

32. T. Xia, M. Lichtman, K. Maller, A. W. Carr, M. J. Piotrowicz, L. Isenhower, and M. Saffman, "Randomized benchmarking of single-qubit gates in a 2D array of neutral-atom qubits," *Phys. Rev. Lett.* **114**, 100503 (2015).

33. Y. Wang, A. Kumar, T.-Y. Wu, and D. S. Weiss, "Single-qubit gates based on targeted phase shifts in a 3D neutral atom array," *Science* **352**, 1562 (2016).

34. M. Saffman and T. G. Walker, "Analysis of a quantum logic device based on dipole-dipole interactions of optically trapped Rydberg atoms," *Phys. Rev. A* **72**, 022347 (2005).

35. T. Wilk, A. Gaëtan, C. Evellin, J. Wolters, Y. Miroshnychenko, P. Grangier, and A. Browaeys, "Entanglement of two individual neutral atoms using Rydberg blockade," *Phys. Rev. Lett.* **104**, 010502 (2010).

36. S. Jandura and G. Pupillo, "Time-optimal two- and three-qubit gates for Rydberg atoms," *Quantum* **6**, 712 (2022).

37. G. Pelegrí, A. J. Daley, and J. D. Pritchard, "High-fidelity multiqubit Rydberg gates via two-photon adiabatic rapid passage," *Quantum Sci. Technol.* **7**, 045020 (2022); see also "High-fidelity Rydberg-blockade entangling gate using shaped, analytic pulses" in this folder.

38. C. Fromonteil, D. Bluvstein, and H. Pichler, "Protocols for Rydberg entangling gates featuring robustness against quasi-static errors," *PRX Quantum* **4**, 020335 (2023).

39. M. Saffman, I. I. Beterov, A. Dalal, E. J. Páez, and B. C. Sanders, "Symmetric Rydberg controlled-Z gates with adiabatic pulses," *Phys. Rev. A* **101**, 062309 (2020).

40. Y.-Y. Jau, A. M. Hankin, T. Keating, I. H. Deutsch, and G. W. Biedermann, "Entangling atomic spins with a Rydberg-dressed spin-flip blockade," *Nat. Phys.* **12**, 71 (2016).

41. W. J. Eckner et al., "Realizing spin squeezing with Rydberg interactions in an optical clock," *Nature* **621**, 734 (2023); see "Spin Squeezing in a Rydberg Lattice Clock" in this folder.

42. L. Isenhower, M. Saffman, and K. Mølmer, "Multibit C_kNOT quantum gates via Rydberg blockade," *Quantum Inf. Process.* **10**, 755 (2011).

43. A. Omran et al., "Generation and manipulation of Schrödinger cat states in Rydberg atom arrays," *Science* **365**, 570 (2019).

44. M. D. Lukin, M. Fleischhauer, R. Côté, L. M. Duan, D. Jaksch, J. I. Cirac, and P. Zoller, "Dipole blockade and quantum information processing in mesoscopic atomic ensembles," *Phys. Rev. Lett.* **87**, 037901 (2001).

45. M. Ebert, A. Gill, M. Gibbons, X. Zhang, M. Saffman, and T. G. Walker, "Atomic Fock state preparation using Rydberg blockade," *Phys. Rev. Lett.* **112**, 043602 (2014).

46. M. Ebert, M. Kwon, T. G. Walker, and M. Saffman, "Coherence and Rydberg blockade of atomic ensemble qubits," *Phys. Rev. Lett.* **115**, 093601 (2015).

47. D. Bluvstein et al., "A quantum processor based on coherent transport of entangled atom arrays," *Nature* **604**, 451 (2022).

48. D. Bluvstein et al., "Logical quantum processor based on reconfigurable atom arrays," *Nature* **626**, 58 (2024).

49. M. Cain et al., "Correlated decoding of logical algorithms with transversal gates," *Phys. Rev. Lett.* **133**, 240602 (2024).

50. S. Ebadi et al., "Quantum optimization of maximum independent set using Rydberg atom arrays," *Science* **376**, 1209 (2022).

51. M. Kwon, M. F. Ebert, T. G. Walker, and M. Saffman, "Parallel low-loss measurement of multiple atomic qubits," *Phys. Rev. Lett.* **119**, 180504 (2017).

52. M. A. Norcia et al., "Midcircuit qubit measurement and rearrangement in a ^{171}Yb atomic array," *Phys. Rev. X* **13**, 041034 (2023).

53. J. W. Lis et al., "Midcircuit operations using the omg architecture in neutral atom arrays," *Phys. Rev. X* **13**, 041035 (2023).